

Trapping the ATP binding state leads to a detailed understanding of the F_1 -ATPase mechanism

Kwangho Nam^{a,b,1,2}, Jingzhi Pu^{a,c,1,2}, and Martin Karplus^{a,d,2}

^aDepartment of Chemistry and Chemical Biology, Harvard University, Cambridge, MA 01238; ^bDepartment of Chemistry and Computational Life Science Cluster, Umeå University, 901 87, Umeå, Sweden; ^cDepartment of Chemistry and Chemical Biology, Indiana University-Purdue University Indianapolis, Indianapolis, IN 46202; and ^dLaboratoire de Chimie Biophysique, Institut de Science et d'Ingénierie Supramoléculaires, Université de Strasbourg, 67000 Strasbourg, France

Contributed by Martin Karplus, October 10, 2014 (sent for review June 26, 2014)

The rotary motor enzyme F_0F_1 -ATP synthase uses the proton-motive force across a membrane to synthesize ATP from ADP and P_i ($H_2PO_4^-$) under cellular conditions that favor the hydrolysis reaction by a factor of 2×10^5 . This remarkable ability to drive a reaction away from equilibrium by harnessing an external force differentiates it from an ordinary enzyme, which increases the rate of reaction without shifting the equilibrium. Hydrolysis takes place in the neighborhood of one conformation of the catalytic moiety F_1 -ATPase, whose structure is known from crystallography. By use of molecular dynamics simulations we trap a second structure, which is rotated by 40° from the catalytic dwell conformation and represents the state associated with ATP binding, in accord with single-molecule experiments. Using the two structures, we show why P_i is not released immediately after ATP hydrolysis, but only after a subsequent 120° rotation, in agreement with experiment. A concerted conformational change of the $\alpha_3\beta_3$ crown is shown to induce the 40° rotation of the γ -subunit only when the β_E subunit is empty, whereas with P_i bound, β_E serves as a latch to prevent the rotation of γ . The present results provide a rationalization of how F_1 -ATPase achieves the coupling between the small changes in the active site of β_{DP} and the 40° rotation of γ .

F_1 -ATPase | chemomechanical coupling | ATP waiting state | molecular dynamics | P_i release

The molecular motor F_0F_1 -ATP synthase is composed of two domains: a transmembrane portion (F_0), the rotation of which is induced by a proton gradient, and a globular catalytic moiety (F_1) that synthesizes and hydrolyzes ATP. The primary function of the proton-motive force acting on F_0F_1 -ATP synthase is to provide the torque required to rotate the γ -subunit in the direction for ATP synthesis (1, 2). The catalytic moiety, F_1 -ATPase, has an $\alpha_3\beta_3$ “crown” composed of three α - and three β -subunits arranged in alternation around the γ -subunit, which has a globular base and an extended coiled-coil portion (3) (Fig. 1A). F_1 -ATPase by itself binds ATP and hydrolyzes it to induce rotation of the γ -subunit (in the opposite direction from that for synthesis) on the millisecond time scale under optimum conditions (4, 5). All of the α - and β -subunits bind nucleotides, but only the three β -subunits are catalytically active. The original crystal structure (3) of F_1 -ATPase from bovine heart mitochondria (MF₁) led to the identification of three conformations of the β -subunit: β_E (empty), β_{TP} (ATP analog bound), and β_{DP} (ADP bound); Fig. 1A. In the known structures of F_1 -ATPase, which apparently are near the “catalytic dwell” state, the state in which catalysis occurs (6, 7), the β_E subunit conformation is partly to fully open and is very different from those of the β_{TP} and β_{DP} subunits, which are closed and very similar to each other (SI Appendix, S11).

Searching for the ATP Waiting State

Because no X-ray structure is available for the ATP waiting state, we searched for it by molecular dynamics (MD) simulations with an external torque applied to the γ -subunit in the hydrolysis

direction while introducing different conformations of the β_{DP} subunit in the $\alpha_3\beta_3$ crown, in accord with suggestions from single-molecule experiments (8). The results are shown in Fig. 2 (see *Methods* and SI Appendix, S12 for details of the simulations). In Fig. 2, we refer 200° for the γ -rotation angle of the catalytic dwell state and 240° for the ATP waiting dwell state, respectively, to stress that the hydrolysis of an ATP, denoted as ATP*, bound after the ATP waiting dwell at 0° , takes place at the 200° catalytic dwell state (see Fig. 1B for the rotation angle of γ relative to the $\alpha_3\beta_3$ complex). The initial simulation used the “Walker” crown structure [Protein Data Bank (PDB) ID code 1BMF] (3), in which the β_{DP} subunit is closed with the angle ($B^{\wedge}C$) formed by helices B and C equal to 21.6° , and the γ -subunit structure of Gibbons et al. (PDB ID code 1E79) (9) (Fig. 1; see *Methods* for system preparation). It was represented by an all-atom model based on the CHARMM program (10), combined with a coarse-grained plastic network model (PNM) (11, 12). Even for an applied torque of 2,500 pN-nm, much higher than is generated in the normal function (13), the γ -subunit, which has an initial rotation angle of 200° , stalled at an angle of about 220° . In the present work, we define the rotation angle of γ as the angle formed between an instantaneous vector and a reference vector, each defining the orientation of γ relative to the three β -subunits for the instantaneous configuration from MD or the reference Walker structure, respectively (see *Methods* and SI Appendix, S12 for angle definition). Major clashes between residues γ S12-I16 and β_{DP} L384-I388, near the DELSEED motif, prevented further rotation (SI Appendix, S13 and Fig. S1). When the external torque was removed, the γ -subunit returned to within 2.5° of the crystal

Significance

F_1 -ATPase is a motor protein that converts the free energy of binding of ATP and its hydrolysis products ADP and P_i into a mechanical force for γ -subunit rotation. It is the catalytic moiety of F_0F_1 -ATPase, which synthesizes ATP. There are two metastable states along each 120° rotation of the γ -subunit, one associated with ATP hydrolysis (the “catalytic dwell”) and the other with ATP binding (the “ATP waiting dwell”). We use molecular simulations to determine the ATP waiting dwell structure. With this structure and the catalytic dwell X-ray structure, we develop an atomic-level model of the coupling between ATP hydrolysis and γ -subunit rotation. The molecular-level understanding of this motor will aid in its use in nanomachines and cancer therapy.

Author contributions: K.N., J.P., and M.K. designed research; K.N. and J.P. performed research; K.N., J.P., and M.K. analyzed data; and K.N., J.P., and M.K. wrote the paper.

The authors declare no conflict of interest.

¹K.N. and J.P. contributed equally to this work.

²To whom correspondence may be addressed. Email: kwangho.nam@chem.umu.se, jpu@iupui.edu, or marci@tammy.harvard.edu.

This article contains supporting information online at www.pnas.org/lookup/suppl/doi:10.1073/pnas.1419486111/-DCSupplemental.

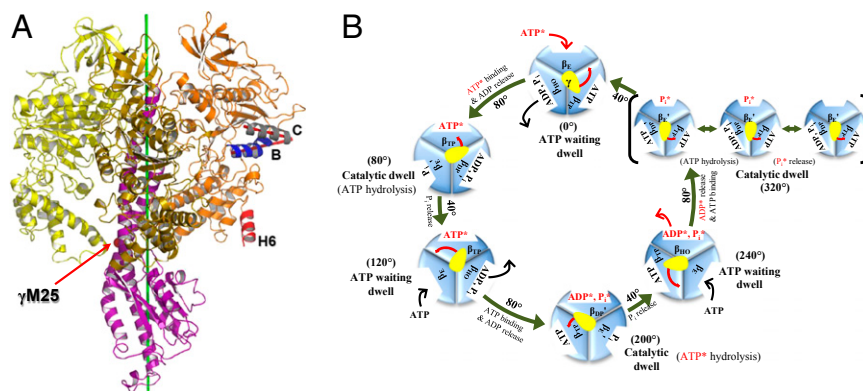


Fig. 1. (A) F_1 -ATPase. The three β -subunits and the γ -subunit are shown (α -subunits are not shown for clarity): β_E (yellow), β_{DP} (orange), β_{TP} (gold), and γ (purple). To define the β_{DP} subunit conformation we use the angle between helix B (β T163-A176) and helix C (β T190-G204). The two helices are highlighted: helix B (blue) and helix C (gray); the B^C angle is depicted as a red angle. The β_{DP} H6 helix, whose orientation was reported to undergo a 20° change during the 40° substep γ -rotation, is highlighted as red. During the forced rotation simulations with an external torque, the force acts on the C_α atom of MF $_1$: γ M25 (shown as a red sphere). The direction of the force is determined as the cross-product of the radial vector of γ M25: C_α and the rotational axis (green). (B) Proposed 360° rotation cycle of F_1 -ATPase showing the subunit conformations, as well as the binding–release of ligands and the hydrolysis of ATP. Starting from the binding of an ATP* to the β_E subunit in the ATP waiting state (0°), rotation of the γ -stalk by 200° (80° , 40° , 80°) leads to the transition of β_E ($\gamma = 0^\circ$) via β_{TP} ($\gamma = 80^\circ$) to β_{DP} ($\gamma = 200^\circ$), the catalytic dwell state where hydrolysis of ATP* takes place. The hydrolysis product P_i^* in the β_{DP} subunit is not released at this catalytic dwell (200°). Instead, the other hydrolysis product ADP* is released first after a 40° rotation [β_{DP} (200°) \rightarrow β_{HO} (240°)]. Then, β_{HO} is transformed to β_E and P_i^* is released after an additional 80° rotation to another catalytic dwell state (320°); the latter is shown in brackets outside the main cycle (see below). Finally, the release of P_i^* from β_E leads to a 40° rotation that completes the 360° cycle (21, 41). The other subunits are going through corresponding cycles offset by 120° (β_{DP}) and 240° (β_{TP}), respectively. Here, the prime symbol when it appears on the β_{DP} and β_E conformations indicates that the conformation of corresponding subunits change slightly in or near the specified reaction steps. The γ -subunit is shown as a yellow oval, and its rotation during the hydrolysis cycle is indicated by a red arrow. The reaction steps occurring in or near the catalytic dwell and corresponding changes of ligands in each β -subunit are also shown in the 320° catalytic dwell: The first state (Left in the 320° catalytic dwell) has a bound ATP in β_{DP}' , and is thus referred to as a prehydrolysis state (the state before the hydrolysis of ATP during the catalytic dwell). The second state (Middle) represents the state after ATP hydrolysis (posthydrolysis state), and the third state (Right) presents the state after the release of P_i bound in β_E' (postrelease state).

orientation in 200 ps, indicating that for the Walker crown structure, the γ -subunit orientation (200°) is a minimum.

To find the ATP waiting state, we restarted the external torque simulations with more open conformations for the β_{DP} subunit, keeping the rest of the crown near its original structure with the PNM. Fig. 2 shows the γ -rotation angle and the (B^C) angle of β_{DP} along the simulated conformational transition of β_{DP} to the more open conformation in the presence of the external torque. For a slightly more open β_{DP} subunit ($B^C = 28^\circ$), similar to that of the half-open β_{HO} conformation ($B^C = 23^\circ$; PDB ID code 2HLD_I, where “I” denotes the first $\alpha_3\beta_3\gamma$ -complex among the three complexes in the crystallographic asymmetric unit of 2HLD) (14), the γ -subunit returned to fluctuate around 202° . With the β_{DP} subunit having B^C equal to 31° and 35° , similar to that of the half-closed β_{HC} conformation ($B^C = 32^\circ$) (see also below) in the Menz et al. structure (PDB ID code 1H8E) (15), the γ -subunit rotated to 255° and 271° , respectively, before it stalled again. When the torque was removed, the γ -subunit relaxed rapidly in both cases to near 240° and remained there during the rest of the simulation. The results show that there exists a locally stable state with the γ -rotation angle near 240° and the $\alpha_3\beta_3$ crown with the catalytic subunits having conformations corresponding to β_E -like, β_{HC} -like (based on the B^C angle), and β_{TP} -like. We note that the B^C angles are $\beta_E = 49^\circ$, $\beta_{HC} = 32^\circ$, $\beta_{HO} = 23^\circ$, $\beta_{DP} = 22^\circ$, and $\beta_{TP} = 19^\circ$.

To check the trapping simulation, we used an alternative protocol (SI Appendix, SI2) and experimental data from Masaïke et al. (8), who estimated that the helix-6 angle of β_{DP} is rotated by 20° in the ATP waiting state. The β_{DP} subunit and the γ -subunit were subjected to a biased simulation (16) and it was found that for the partly open structure of β_{DP} (helix-6 angle equal 20° ; $B^C = 23^\circ$) the γ -subunit had rotated by 40° to reach the 240° state. A number of interactions stabilize the 240° state (see Fig. 3 and SI Appendix, SI4 for details and a comparison with the interactions in the trapped structure). The structure was then subjected to all-

atom explicit water MD simulations with no PNM (see SI Appendix, SI5 for details). Throughout the simulation (20 ns), the γ -stalk stayed near 240° , supporting the fact that it is a (locally) stable state. In SI Appendix, Fig. S2 A and B, we show the structure from the simulation, and compare it with the structure at the catalytic dwell. The conformations of β_{DP} for the two states differ as expected. Comparisons of β_{DP} with various

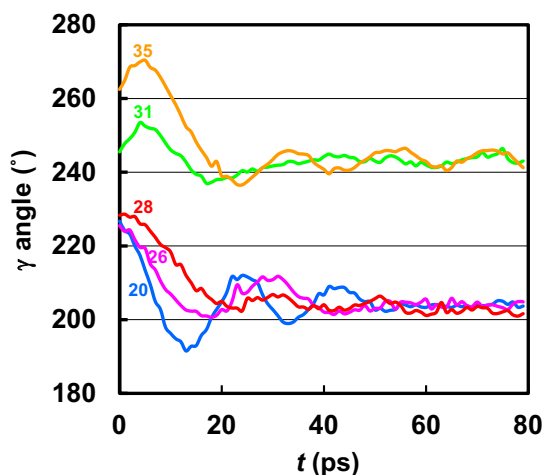
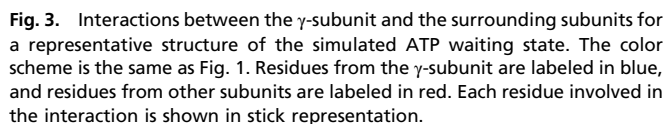


Fig. 2. Rotational angle of the γ -subunit as a function of time during the relaxation simulations (see text) for different B^C angle values of the β_{DP} subunit after the simulations with the applied torque. The values of the B^C angle in the β_{DP} subunit are shown for each trajectory to indicate the stage of binding left opening during the transition from the β_{DP} ($B^C = 21.6^\circ$) to the β_E ($B^C = 48.6^\circ$) conformation. The B^C angles were maintained at their initial values by the PNM restraining potentials during the simulations.



PNAS | December 16, 2014 | vol. 111 | no. 50 | 17853

P_i release from β -subunits in different conformational states as a function of the temperature of the multiple copies of P_i . In the Braig et al. structure used for the catalytic dwell state (200°), β_E is occupied by P_i ; β_{DP} by ADP, AlF_3 (which was replaced with P_i), and Mg^{2+} ; and β_{TP} by ATP analog and Mg^{2+} . The P_i present in β_E was produced during the catalytic dwell at 80° from an ATP bound at -120° . Because P_i has a high release probability from β_E at a temperature as low as 250 K, it is very weakly bound. Interestingly, in one of the all-atom explicit water MD simulations (see below), we observed the spontaneous release and rebinding of P_i from β_E (Movie S1). The release and rebinding accompany a large fluctuation of the P-loop structure. This finding is consistent with the present P_i release data. By contrast, a much higher temperature (1,500 K) is required for a significant release probability of P_i from the closed β_{DP} subunit in the catalytic dwell structure (200°). This result indicates that in the 200° structure, release of P_i from β_E is the dominant process and that release of P_i^* from β_{DP} immediately after its cleavage from ATP* does not occur to a significant extent, in accord with Fig. 1*B* and the proposal of Watanabe et al. (21).

In the ATP waiting state (240°), where β_E is empty (Fig. 1*B*), β_{DP} has opened more to become β_{HO} , but P_i^* release is even more hindered than in the 200° structure as long as ADP* (and Mg^{2+}) is present (Fig. 1*B*); i.e., release of P_i^* at 240° would be possible only after ADP* has been released (also see *SI Appendix*, *SI7*, *SI8*, and Fig. S4). To confirm this result, we performed a set of MCES simulations for β_{HO} in the 240° structure, in which ADP and P_i were both represented by multiple copies and thus competed for release. As expected, ADP* is released at a significantly lower temperature than P_i^* (Fig. 4). Once ADP* is no longer present, P_i^* is released easily (*SI Appendix*, Fig. S5). However, as shown by Adachi et al. (20) and Martin et al. (27), ADP* is released only during (or after) the rotation of the γ -subunit by another 80° to the catalytic dwell at 320° when β_{HO} has opened further to β_E (see Fig. 1*B* legend). Very recently, Czub and Grubmüller have shown by MD simulations that β_E closes spontaneously to β_{HO} during the 80° rotation in the synthesis direction in the absence of ligand (ADP or P_i) in β_E (28). However, because changes of the ligand occupation of each β -subunit during the rotation were not taken into account in the simulations, an understanding of the entire sequence of events that occurs during the 80° rotation is not possible based on their results. Nevertheless, the results are consistent with the mechanism that the $\beta_{HO} \rightarrow \beta_E$ conformational transition and the rotation of γ to the catalytic dwell occur during or after the release of ADP*. Taken together, the P_i release simulations show that P_i^* is released after the $\beta_{HO} \rightarrow \beta_E$ transition is completed as part of the rotation from 320° to 360° .

Coupling Between ATP Hydrolysis, P_i Release, and γ -Rotation

An essential element for understanding F_1 -ATPase function is knowledge of the mechanism by which the torque for γ -rotation is generated. The dominant factor in the 80° rotation from the waiting dwell is known to be ATP binding to a β_E subunit and its closure to form β_{TP} (12, 29), in which repulsive van der Waals interactions contribute dominantly in the generation of torque. On the other hand, our understanding of the 40° rotation is much more limited (20, 30). To explore the mechanism, we carried out targeted molecular dynamics (TMD) (31) simulations with the model generated in this paper for the ATP waiting structure as the target (see *Methods*). As a reference, a TMD simulation was performed, starting with the catalytic dwell structure, and a perturbation was applied to the γ - and β_{DP} subunits of the entire $\alpha_3\beta_3\gamma$ -complex to induce the 40° rotation of γ and the transition of β_{DP} to β_{HO} required to reach the model ATP waiting structure. The simulation produces a structure with the γ -subunit rotated by 40° and β_{DP} partially open; the structure differs

slightly from the model ATP waiting structure in the orientations of the C-terminal hth motifs of β_E and all of the α -subunits (*SI Appendix*, Fig. S6). The change of the β_E structure during or after the 40° rotation is in accord with the results of Watanabe et al. (30) that in the neighborhood of the ATP waiting state, the affinity for ATP changes with γ -rotation, implying a change in the β_E structure, and the all-atom explicit water MD simulation (*SI Appendix*, Fig. S24). Because the TMD perturbation was applied only to γ and β_{DP} , the structural changes of the other parts of the $\alpha_3\beta_3\gamma$ -complex reflect their spontaneous response to the rotation of γ and the partial opening of β_{DP} . The resulting structure was used as the target structure in subsequent TMD simulations, where the perturbation was applied only to various parts of the $\alpha_3\beta_3$ crown, with or without P_i in the β_E subunit (Fig. 5; see legend for details). With β_E empty, we obtained the striking result that transformations of all α - and β -subunits are required to induce the 40° rotation (Fig. 5). As shown in the figure, when fewer elements of the $\alpha_3\beta_3$ crown are transformed (e.g., all β -subunits), only intermediate rotation of the γ -subunits is produced during the simulation. Moreover, with P_i present in β_E , the P_i stays bound in the active site throughout the entire TMD simulation and only a 10° rotation of γ was achieved even with the full $\alpha_3\beta_3$ transformation in the simulation (Fig. 5, orange; and see *Movies S2* and *S3*). These results show that the presence of P_i in the β_E subunit blocks the γ -rotation.

Dynamic Lock by P_i

To determine the mechanism of the β_E (P_i) lock, the structure and dynamics of the $\alpha_3\beta_3\gamma$ -complex in the catalytic dwell state with different occupations of β_{DP} and β_E were studied by all-atom explicit water MD simulations (see *SI Appendix*, *SI5* for details). In the simulations, the binding pockets of β_{TP} and all α -subunit are occupied by ATP, whereas β_{DP} and β_E have different occupations: In the prehydrolysis state simulation, ATP occupies β_{DP} and P_i occupies β_E ; in the posthydrolysis state simulation, ADP and P_i occupy β_{DP} and P_i occupies β_E ; and in

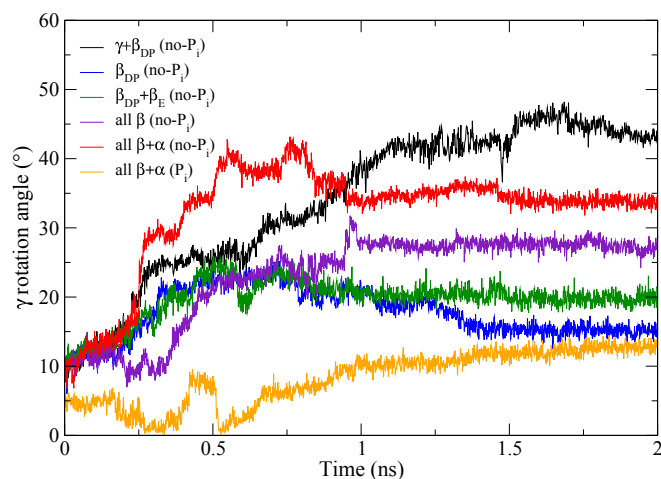


Fig. 5. γ -Rotation angles from the TMD simulations (see text). The no- P_i systems are systems with empty β_E : $\gamma + \beta_{DP}$ simulation (black), β_{DP} simulation (blue), $\beta_{DP} + \beta_E$ simulation (green), all β simulation (purple), all $\beta + \alpha$ simulation (red). For the P_i system, which refers to the system with P_i bound in β_E : all $\beta + \alpha$ simulation (yellow). The simulation time is shown in nanoseconds, and the γ -rotation angle is defined as in Pu and Karplus (12). Except for the $\gamma + \beta_{DP}$ simulation, the TMD simulations continued for 1 ns and were followed by 1-ns unperturbed simulations to relax the system; during the latter all these systems reached a plateau for the rotation angle of γ . In the $\gamma + \beta_{DP}$ TMD simulation, it took 2 ns before the rmsd distance to the 240° rotated structure fell below 0.75 Å; this was followed by a 1-ns relaxation simulation as in the other cases.

the postrelease state simulation, β_{DP} is occupied by ADP and P_i and β_E is empty. (See Fig. 1*B* and its legend for identification of the three states.) The structural comparisons reveal that during or after the hydrolysis of ATP in β_{DP} and the release of P_i from β_E , small changes occur in the C-terminal hth motif and at the intersubunit interfaces of the subunits (*SI Appendix*, Figs. S2*E* and S7, and *Movie S4*). In addition, there are significant differences in the dynamics, as evidenced in the cross-correlation maps of the $\alpha_3\beta_3\gamma$ -complex; they are shown in *SI Appendix*, Fig. S8. Details of the structural and dynamic changes are given below.

SI Appendix, Fig. S8 shows the cross-correlation maps of the entire $\alpha_3\beta_3\gamma$ complex for the prehydrolysis state (*SI Appendix*, Fig. S8*A*), posthydrolysis state (*SI Appendix*, Fig. S8*B*), and the postrelease state (*SI Appendix*, Fig. S8*C*). In comparing the simulation of the posthydrolysis state to that of the prehydrolysis state, there is a rigid-body rotation of the C-terminal hth motif of α_{DP} toward β_{DP} in the former, relative to the latter. This rotation is caused by the cleavage of ATP into ADP and P_i in β_{DP} (*SI Appendix*, Fig. S7*A*). The rotation increases the contact between the two subunits and leads to a more closed α_{DP} - β_{DP} interface, as is evident from the increased buried surface area (*SI Appendix*, Fig. S9). It also leads to enhanced positive cross-correlation between the two subunits without a significant change of the intrasubunit cross-correlation of β_{DP} (compare *SI Appendix*, Fig. S8*A* and *B*). A similar closure of the α_{DP} - β_{DP} interface is observed experimentally. In *SI Appendix*, Fig. S7*B*, the X-ray structure with the transition-state analog (26) is superimposed on the structure with the ATP analog (14). The superposition shows that the C-terminal domain of α_{DP} is rotated toward β_{DP} for the transition-mimic state to make the interface tighter (*SI Appendix*, Fig. S7*B*, *Left*), in agreement with the simulations. The origin of this structural change appears to involve the displacement of α_{DP} R373, which moves to interact with the P_i after it is cleaved from the ATP. *SI Appendix*, Fig. S7*A* shows the displacement of α_{DP} R373 upon the cleavage of ATP in the simulations and a similar displacement in the transition-state mimic structure (*SI Appendix*, Fig. S7*B*; also see *SI Appendix*, Fig. S7*C* for the changes of interactions at the interface between the two subunits). In this interpretation, α_{DP} R373 functions as a sensor that probes the progress of the hydrolysis reaction in β_{DP} and dynamically links the two subunits (β_{DP} and α_{DP}). This is consistent with mutation experiments, which suggested that α_{DP} R373 is involved in the rearrangement of the α_{DP} - β_{DP} interface upon ATP hydrolysis and the catalytic cooperativity of the enzyme (32).

We also find a noticeable difference between the cross-correlation maps of the posthydrolysis and postrelease states, i.e., there is an increase of intrasubunit correlation of both α_E and β_E in the postrelease state (*SI Appendix*, Fig. S8*C*). The cross-correlation maps of α_E and β_E in the postrelease state show cross-correlations that extend over the C-terminal and nucleotide binding domains (*SI Appendix*, Fig. S8*C* and *D*), suggesting that the two domains behave like a rigid body. This difference in the dynamics of β_E is of interest because the differences between the β_E structures with or without P_i or a P_i analog are found to be negligible (*SI Appendix*, S19 and Fig. S10). The anticorrelation between α_E and the C-terminal domain of β_E has also increased significantly (compare *SI Appendix*, Fig. S8*B* and *D*). This result indicates that the two subunits move concertedly but in opposite directions. In this case, α_E R373 could play an important role in controlling the dynamics of α_E and β_E , similar to the role of α_{DP} R373 in ATP hydrolysis. In this mechanism, the interaction between P_i in β_E and α_E R373 keeps α_E close to β_E and away from β_{DP} , preventing α_E from responding to the change of β_{DP} , thus blocking the rotation of γ . Once P_i leaves the binding pocket, the interaction is lost, so that α_E and in particular its C-terminal domain are able to respond to the change occurring in β_{DP} and the rotation of γ .

To test the proposed mechanism, we have performed an additional TMD simulation. The simulation was carried out with the TMD perturbation applied to all α - and β -subunits but without the interaction between P_i in β_E and α_E R373. If these interactions were important in blocking the γ -rotation, it would be expected that γ would rotate further in their absence than when the interactions between P_i in β_E and α_E R373 were present. The simulation produced a γ -rotation that is larger (close to 20°) than the simulation with the P_i - α_E R373 interaction present, but then it falls back to the lower rotation angle during the subsequent relaxation simulation (*SI Appendix*, Fig. S11). The result confirms the proposed role of the interaction between P_i and α_E R373 in blocking γ -rotation. The result also suggests that interactions (within or between β_E and α_E), other than the interactions between P_i in β_E and α_E R373, are important in preventing the rotation—for example, reducing the increase of the intrasubunit cross-correlation in the β_E and α_E subunits and the increase of the anticorrelation between them, which occurs upon the release of P_i . In this regard, we note that α_E is the subunit forming the most extensive surface contacts with γ among the α -subunits and has an extensive surface contact with β_{DP} (*SI Appendix*, Fig. S9). The surface contacts of α_E with γ are as extensive as the contact between β_{DP} and γ , which is the largest surface contact among all β s.

Taken together, the present analysis shows how the interactions between β_E and α_E , including the interaction between P_i and α_E R373, act as a “dynamic lock” to keep the protein in the prerotated catalytic dwell state. Only after P_i in β_E is released is α_E freed from β_E and able to fully engage with β_{DP} to complete the concerted conformational transition of the $\alpha_3\beta_3$ complex by which the γ -subunit rotates to reach the ATP waiting dwell state. Such dynamic locks have been proposed for different systems by Laity et al. for zinc finger proteins (33) and by Young et al. for c-Src (34).

Concluding Remark

The present study provides a structural model for the ATP waiting state of F_1 -ATPase, in agreement with single-molecule experiments which have suggested that it does not coincide with any of the known crystal structures. Knowledge of this structure, combined with that of the state in which catalysis takes place, makes possible the development of a detailed atomic-level description of the coupling between the binding and hydrolysis of ATP and the γ -subunit rotation induced by the conformational changes of the α - and β -subunits. The suggested tests of the proposal structure and a possible method for trapping it in a crystallographically accessible conformation should stimulate experimental studies (see *SI Appendix*, S110 and S111 for details).

Methods

Forced Rotation Simulation for Finding the ATP Waiting State. The structure of the minimal rotary complex $\alpha_3\beta_3\gamma$ was prepared based on the $\alpha_3\beta_3$ subcomplex of the 1BMF structure (3) and the γ -subunit of the 1E79 structure (9) by a procedure similar to that of Ma et al. (35). The CHARMM19 all-atom force field (36) and the EEF1 implicit solvation model (37) were used to describe the protein system and water solvation, respectively. In addition, the coarse-grained PNM (11, 12), in which each PNM node was assigned to the corresponding C_α atom position of the protein, was used to stabilize the protein conformation in the presence of the high forces used in the simulation. The system was first heated from 0 K to 300 K in 60 ps and then equilibrated at 300 K for 300 ps (see details in *SI Appendix*, S12). The MD simulations were carried out with a 2-fs integration time step and SHAKE (38) applied to the bonds involving hydrogen atoms. The temperature was controlled using the Langevin thermostat.

After equilibration at 300 K for 300 ps, a large external torque was applied to drive the rotation of the γ -subunit in the hydrolysis direction (counterclockwise as seen from the membrane). Using the PULL command of the CHARMM program (10), an external force of 2,500 pN was applied to the C_α

atom of residue γ M25. Residue γ M25 was identified by Pu and Karplus to provide a key contact point for the torque generation (12). In the forced rotation simulation, the external torque was applied only when backward rotation is detected. In that way, the simulation was biased toward the hydrolysis direction only when γ rotates backward but not when the forward rotation occurs spontaneously; the γ -rotation angle was checked at each update step (at every 1 ps). The γ -rotation angle is defined as in Pu and Karplus (12) using the $\alpha_3\beta_3$ (1BMF)– γ (1E79) Walker structure as the reference structure for the catalytic dwell state, and a similar definition was used in the work by Koga and Takada (39). The direction of the force was determined as the instantaneous cross-product between the radial vector of the residue γ M25 (perpendicular to the rotational axis) and the rotational axis itself (Fig. 1A). See *SI Appendix, S12* for details of forced rotation simulations and definition of the γ -rotation angle.

P_i Release Simulations. The 200° rotated system was prepared using the $\alpha_3\beta_3$ subcomplex of the 1E1R structure (26) and the γ -subunit from the 1E79 structure (9). For the 240° state, the starting structure was the present ATP waiting state model structure. For the P_i release MCES simulation (25), the P_i molecule was replicated 30 times by using the BLOCK module of the CHARMM program. In all simulations, P_i was treated as doubly protonated ($H_2PO_4^-$), which was found to be favored in the active site of β -subunit (40). The interaction between the multiply copied P_i and both the protein and the solvent was scaled by a factor that is inversely proportional to the number of P_i copies, whereas each P_i has no interaction with other P_i molecules. The remaining interactions were not scaled. The temperature of P_i was controlled by attaching each P_i to a separate Langevin thermostat, while the remainder of the system was maintained at 300 K. At each P_i temperature, the MCES simulation was repeated 40 times (*SI Appendix, S17*). Each

simulation was started with different initial velocities and ran for 2 ns with a 1-fs integration time step. SHAKE was applied to constrain bonds involving hydrogen atoms.

Targeted MD Simulations of the Coordinated Conformational Transition of the $\alpha_3\beta_3\gamma$ -Complex. The 40° substep rotation was simulated by applying the TMD simulation method (31). The TMD simulation was first carried out with the 200° rotated catalytic dwell structure, which was prepared for the MCES P_i release simulations. The TMD perturbation was applied to the nonhydrogen atoms of the γ - and β_{DP} subunits of the entire $\alpha_3\beta_3\gamma$ -complex for the $\beta_{DP} \rightarrow \beta_{HO}$ transition and the 40° γ rotation; the ATP waiting model structure was the target structure. Subsequently, using this TMD-produced structure as the target structure for the $\alpha_3\beta_3$ complex, a set of TMD simulations was carried out with the TMD perturbation applied to various parts of the $\alpha_3\beta_3$ crown with or without P_i in β_E and without any perturbation to γ (see Fig. 5 legend for the notation of each TMD simulation). In the simulations the rmsd distance to the target structure was decreased by 0.2×10^{-6} Å at each MD step until the rmsd distance reached a value lower than 0.75 Å.

ACKNOWLEDGMENTS. We are grateful to members of the M.K. group for helpful discussions and Dr. Gerhard Hummer for providing the coordinates of their modeled F_1 -ATPase structure. The work was supported in part by a grant from the National Institutes of Health (M.K.) and by a start-up grant from Indiana University-Purdue University Indianapolis (J.P.) and from Umeå University (K.N.). The computational resources were provided by the National Energy Research Scientific Computing Center, Faculty of Arts and Science Division Research Computing Group at Harvard University, and the Swedish National Infrastructure for Computing at High Performance Computing Center North (HPC2N).

- Itoh H, et al. (2004) Mechanically driven ATP synthesis by F_1 -ATPase. *Nature* 427(6973):465–468.
- Walker JE (2013) The ATP synthase: The understood, the uncertain and the unknown. *Biochem Soc Trans* 41(1):1–16.
- Abrahams JP, Leslie AGW, Lutter R, Walker JE (1994) Structure at 2.8 Å resolution of F_1 -ATPase from bovine heart mitochondria. *Nature* 370(6491):621–628.
- Karplus M, Gao YQ (2004) Biomolecular motors: The F_1 -ATPase paradigm. *Curr Opin Struct Biol* 14(2):250–259.
- Spetzler D, et al. (2006) Microsecond time scale rotation measurements of single F_1 -ATPase molecules. *Biochemistry* 45(10):3117–3124.
- Yasuda R, et al. (2003) The ATP-waiting conformation of rotating F_1 -ATPase revealed by single-pair fluorescence resonance energy transfer. *Proc Natl Acad Sci USA* 100(16):9314–9318.
- Okuno D, et al. (2008) Correlation between the conformational states of F_1 -ATPase as determined from its crystal structure and single-molecule rotation. *Proc Natl Acad Sci USA* 105(52):20722–20727.
- Masaika T, Koyama-Horibe F, Oiwa K, Yoshida M, Nishizaka T (2008) Cooperative three-step motions in catalytic subunits of F_1 -ATPase correlate with 80° and 40° substep rotations. *Nat Struct Mol Biol* 15(12):1326–1333.
- Gibbons C, Montgomery MG, Leslie AGW, Walker JE (2000) The structure of the central stalk in bovine F_1 -ATPase at 2.4 Å resolution. *Nat Struct Biol* 7(11):1055–1061.
- Brooks BR, et al. (2009) CHARMM: The biomolecular simulation program. *J Comput Chem* 30(10):1545–1614.
- Maragakis P, Karplus M (2005) Large amplitude conformational change in proteins explored with a plastic network model: Adenylate kinase. *J Mol Biol* 352(4):807–822.
- Pu J, Karplus M (2008) How subunit coupling produces the γ -subunit rotary motion in F_1 -ATPase. *Proc Natl Acad Sci USA* 105(4):1192–1197.
- Noji H, Yasuda R, Yoshida M, Kinosita K, Jr (1997) Direct observation of the rotation of F_1 -ATPase. *Nature* 386(6622):299–302.
- Kabaleeswaran V, Puri N, Walker JE, Leslie AGW, Mueller DM (2006) Novel features of the rotary catalytic mechanism revealed in the structure of yeast F_1 ATPase. *EMBO J* 25(22):5433–5442.
- Menz RI, Walker JE, Leslie AGW (2001) Structure of bovine mitochondrial F_1 -ATPase with nucleotide bound to all three catalytic sites: Implications for the mechanism of rotary catalysis. *Cell* 106(3):331–341.
- Paci E, Karplus M (1999) Forced unfolding of fibronectin type 3 modules: An analysis by biased molecular dynamics simulations. *J Mol Biol* 288(3):441–459.
- Rees DM, Montgomery MG, Leslie AGW, Walker JE (2012) Structural evidence of a new catalytic intermediate in the pathway of ATP hydrolysis by F_1 -ATPase from bovine heart mitochondria. *Proc Natl Acad Sci USA* 109(28):11139–11143.
- Okazaki K, Hummer G (2013) Phosphate release coupled to rotary motion of F_1 -ATPase. *Proc Natl Acad Sci USA* 110(41):16468–16473.
- Ross J (2006) Energy transfer from adenosine triphosphate. *J Phys Chem B* 110(13):6987–6990.
- Adachi K, et al. (2007) Coupling of rotation and catalysis in F_1 -ATPase revealed by single-molecule imaging and manipulation. *Cell* 130(2):309–321.
- Watanabe R, Iino R, Noji H (2010) Phosphate release in F_1 -ATPase catalytic cycle follows ADP release. *Nat Chem Biol* 6(11):814–820.
- Junge W, Sielaff H, Engelbrecht S (2009) Torque generation and elastic power transmission in the rotary F_0F_1 -ATPase. *Nature* 459(7245):364–370.
- Shimo-Kon R, et al. (2010) Chemo-mechanical coupling in F_1 -ATPase revealed by catalytic site occupancy during catalysis. *Biophys J* 98(7):1227–1236.
- Elber R, Karplus M (1990) Enhanced sampling in molecular dynamics: Use of the time-dependent Hartree approximation for a simulation of carbon monoxide diffusion through myoglobin. *J Am Chem Soc* 112(25):9161–9175.
- Cecchini M, Alexeev Y, Karplus M (2010) P_i release from myosin: A simulation analysis of possible pathways. *Structure* 18(4):458–470.
- Braig K, Menz RI, Montgomery MG, Leslie AGW, Walker JE (2000) Structure of bovine mitochondrial F_1 -ATPase inhibited by Mg^{2+} ADP and aluminium fluoride. *Structure* 8(6):567–573.
- Martin JL, Ishmukhametov R, Hornung T, Ahmad Z, Frasch WD (2014) Anatomy of F_1 -ATPase powered rotation. *Proc Natl Acad Sci USA* 111(10):3715–3720.
- Czub J, Grubmüller H (2014) Rotation triggers nucleotide-independent conformational transition of the empty β subunit of F_1 -ATPase. *J Am Chem Soc* 136(19):6960–6968.
- Yasuda R, Noji H, Yoshida M, Kinosita K, Jr, Itoh H (2001) Resolution of distinct rotational substeps by submillisecond kinetic analysis of F_1 -ATPase. *Nature* 410(6831):898–904.
- Watanabe R, et al. (2012) Mechanical modulation of catalytic power on F_1 -ATPase. *Nat Chem Biol* 8(1):86–92.
- Schlitter J, Engels M, Krüger P, Jacoby E, Wollmer A (1993) Targeted molecular dynamics simulation of conformational change—Application to the T \leftrightarrow R transition in insulin. *Mol Simul* 10:291–308.
- Senior AE, Nadanaciva S, Weber J (2002) The molecular mechanism of ATP synthesis by F_1F_0 -ATP synthase. *Biochim Biophys Acta* 1553(3):188–211.
- Laity JH, Dyson HJ, Wright PE (2000) DNA-induced α -helix capping in conserved linker sequences is a determinant of binding affinity in Cys2–His2 zinc fingers. *J Mol Biol* 295(4):719–727.
- Young MA, Gonfloni S, Superti-Furga G, Roux B, Kuriyan J (2001) Dynamic coupling between the SH2 and SH3 domains of c-Src and Hck underlies their inactivation by C-terminal tyrosine phosphorylation. *Cell* 105(1):115–126.
- Ma J, et al. (2002) A dynamic analysis of the rotation mechanism for conformational change in F_1 -ATPase. *Structure* 10(7):921–931.
- Brooks BR, et al. (1983) CHARMM: A program for macromolecular energy, minimization, and dynamics calculations. *J Comput Chem* 4:187–217.
- Lazaridis T, Karplus M (1999) Effective energy function for proteins in solution. *Proteins* 35(2):133–152.
- Ryckaert J-P, Ciccotti G, Berendsen HJC (1977) Numerical integration of the Cartesian equations of motion of a system with constraints: Molecular dynamics of n-alkanes. *J Comput Phys* 23:327–341.
- Koga N, Takada S (2006) Folding-based molecular simulations reveal mechanisms of the rotary motor F_1 -ATPase. *Proc Natl Acad Sci USA* 103(14):5367–5372.
- Yang W, Gao YQ, Cui Q, Ma J, Karplus M (2003) The missing link between thermodynamics and structure in F_1 -ATPase. *Proc Natl Acad Sci USA* 100(3):874–879.
- Gao YQ, Yang W, Karplus M (2005) A structure-based model for the synthesis and hydrolysis of ATP by F_1 -ATPase. *Cell* 123(2):195–205.